THE JOURNAL OF BIOLOGICAL CHEMISTRY VOL. 286, NO. 35, pp. 30859–30866, September 2, 2011

A Conserved Structural Determinant Located at the Interdomain Region of Mammalian Inositol-requiring Enzyme 1α*[S]

Received for publication, June 19, 2011, and in revised form, July 7, 2011 Published, JBC Papers in Press, July 13, 2011, DOI 10.1074/jbc.M111.273714

Zhen Xue[‡§], Yin He[¶], Kaixiong Ye[‡§], Zhenglong Gu[‡§¶], Yuxin Mao[‖], and Ling Qi[‡§¶1]

From the [‡]Graduate Program in Nutrition, the [¶]Graduate Program in Genetics and Development, and the [§]Division of Nutritional Sciences, Cornell University, Ithaca, New York 14853 and the [‖]Weill Institute of Molecular and Cell Biology, Department of Molecular Biology and Genetics, Cornell University, Ithaca, New York 14853

Inositol-requiring enzyme 1α (IRE1α), an endoplasmic reticulum-resident sensor for mammalian unfolded protein response, is a bifunctional enzyme containing kinase and RNase domains critical for trans-autophosphorylation and *Xbp1* mRNA splicing, respectively, in response to endoplasmic reticulum stress. However, the amino acid residues important for its function and activation remain largely unexplored. Here, through analysis of IRE1α mutants associated with human somatic cancers, we have identified a highly conserved proline residue at position 830 (Pro^{830}) that is critical for its structural integrity and hence, the activation of both kinase and RNase domains. Structural analysis revealed that Pro^{830} may form a highly conserved structural linker with adjacent tryptophan and tyrosine residues at positions 833 and 945 (Trp^{833} and Tyr^{945}), thereby bridging the kinase and RNase domains. Indeed, mutation of Pro^{830} to leucine (P830L) completely abolished the kinase and RNase activities, significantly decreased protein stability, and prevented oligomerization of IRE1α upon ER stress; similar observations were made for mutations of Trp^{833} to alanine (W833A) and to a lesser extent for Y945A. Our finding may facilitate the identification of small molecules to compromise IRE1α function specifically.

The unfolded protein response (UPR),[2] a highly conserved endoplasmic reticulum (ER)-to-nucleus signaling pathway is critical for maintaining ER homeostasis and has been implicated in the pathogenesis of many human diseases, including diabetes, cancer, and lung and heart diseases. UPR is initiated by the activation of three major sensors at the ER membrane: inositol-requiring enzyme 1 (IRE1), PKR-like-ER kinase, and activating transcription factor 6. Activation of UPR leads to the induction of chaperones, and ER-associated degradation components, global translational attenuation, is required for the maintenance of ER function, clearance of misfolded proteins from the ER, and if stress persists, induction of apoptosis (1). Among the three branches, the IRE1α-initiated pathway is the most evolutionarily conserved and represents the only UPR in yeast (2, 3). Recent studies have shown that this pathway plays important roles in a wide range of physiological and disease conditions including B cell and adipocyte differentiation, secretory function for pancreas and salivary glands, neurodegeneration, and obesity and insulin resistance (1, 4). Hence, a comprehensive understanding of the regulatory mechanisms underlying mammalian IRE1α activation is critical to the development of new therapeutic approaches.

In addition to a kinase domain, the cytoplasmic tail of the IRE1α protein also possesses endoribonuclease (RNase) activity which cleaves *Hac1*/*Xbp1* mRNA (5, 6). The *Hac1*/*Xbp1* mRNA encodes a potent transcription factor responsible for the up-regulation of many genes involved in protein folding, degradation and trafficking (7–10). The ER luminal domain of IRE1α protein is critical for sensing ER stress and subsequent IRE1α activation. Although earlier studies of human IRE1α have suggested that IRE1α dimers are sufficient for its activity (11–14), recent studies showed that the formation of stress-induced IRE1α foci is conserved between yeast and mammals (15, 16). The formation of IRE1α foci in response to ER stress is believed to juxtapose the IRE1α kinase and RNase domains, thereby allowing for a more efficient way to relay signals emanating from the ER lumen.

One outstanding question is the importance of and the molecular mechanism underlying the activation of mammalian IRE1α RNase and kinase domains. Some recent studies have shed light on this question. First, kinase-defective K599A mutant abolishes the RNase activity of IRE1α, suggesting that kinase activity and trans-autophosphorylation of IRE1α protein are important for the activation of its RNase domain (15). This is likely achieved by phosphorylation-induced conformational changes. Moreover, a previous study reported the failure to express stable forms of individual kinase and RNase domains (18). Together, these studies imply that the two cytosolic domains of IRE1α protein are functionally linked via autophosphorylation. However, two recent studies suggested a dispensable role of IRE1α phosphorylation in activation of its RNase domain (19, 20). Thus, further studies are required to elucidate the relationship between these two domains.

* This work was supported, in whole or in part, by NIDDK, National Institutes of Health Grant R01DK082582 (to L. Q.). This work was also supported by Cornell startup packages (to L. Q., Z. G., and Y. M.) American Diabetes Association Grant 7-08-JF-47 (to L. Q.).

[S] The on-line version of this article (available at http://www.jbc.org) contains supplemental Figs. S1 and S2.

[1] To whom correspondence should be addressed. Tel.: 607-254-8857; Fax: 607-255-6249; E-mail: lq35@cornell.edu.

[2] The abbreviations used are: UPR, unfolded protein response; ER, endoplasmic reticulum; IRE1α, inositol-requiring enzyme 1α; MEF, mouse embryonic fibroblast; Tg, thapsigargin.

A

Tissue	Histology/type	cDNA annotation	AA annotation	Location
Renal	Clear cell carcinoma	A731G	N244S	ER lumen
Lung	Adenocarcinoma	T1421G	L474R	Cytosol (linker)
Stomach	Adenocarcinoma	C1903T	R635W	Cytosol (Kinase)
Brain	Glioblastoma	C2306T	S769F	Cytosol (Kinase)
Brain	Glioblastoma	C2338T	Q780* (STOP)	Cytosol (Kinase)
Ovary	Serous carcinoma	C2489T	P830L	Cytosol (Kinase)

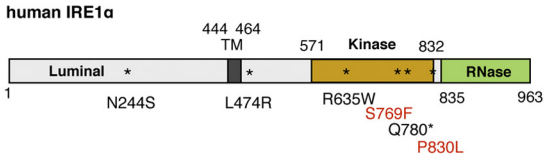

B

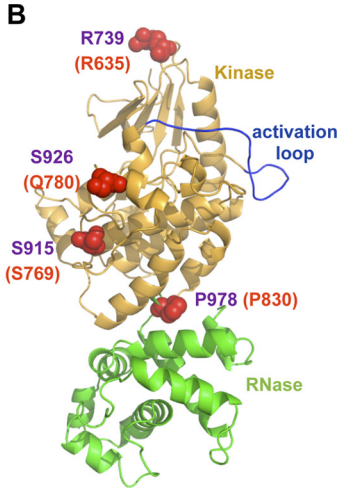

FIGURE 1. **Distribution of IRE1α mutations associated with human cancers.** *A*, list of mutations identified in human cancers (*upper*) and their distribution in human IRE1α (*lower*). Mutations that abolish IRE1α activity are highlighted in *red*. *Luminal*, luminal domain; *TM*, transmembrane; *Kinase*, kinase domain; and *RNase*, RNase domain of human IRE1α. *B*, location of four human mutations (*red*) in the kinase domain of yeast IRE1 protein based on homology (*purple*). Kinase domain is in *orange*, RNase domain in *green*, and activation loop in *blue* as shown.

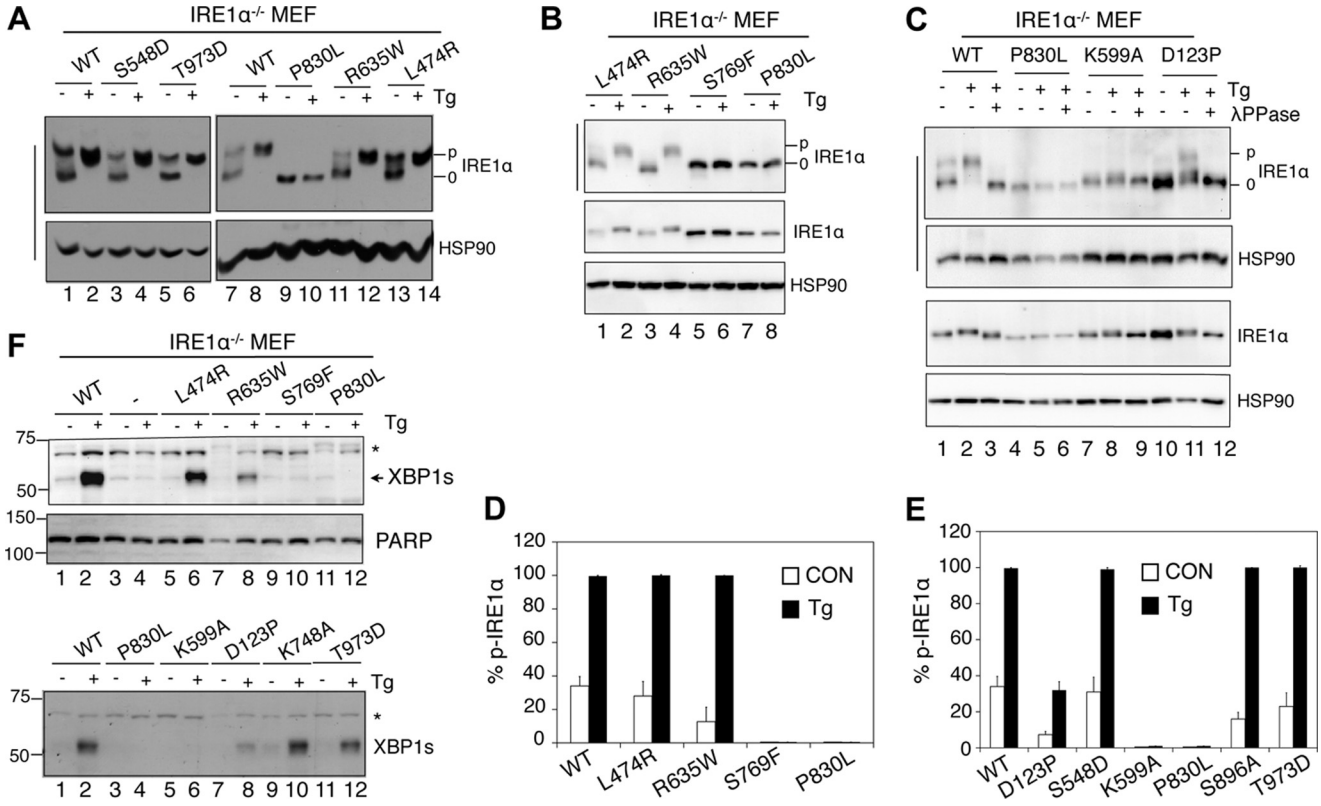

FIGURE 2. **The P830L mutation abolishes IRE1α phosphorylation and activation.** *A–C*, Western blot analysis of IRE1α in cell lysates of IRE1α$^{-/-}$ MEFs stably expressing WT or mutant IRE1α. Cells were treated with 60 nM Tg for 3 h. In *C*, lysates were treated with λPPase. Phos-tag gels are indicated with a *straight line* on the *left side*. HSP90, a loading control. Note the difference of IRE1α pattern in Phos-tag gels *versus* regular SDS-polyacrylamide gels. *D* and *E*, quantitation of *p*-IRE1α in Phos-tag gels shown in *A–C*. Results are expressed as mean ± S.E. (*error bars*). All *p* values <0.05 used unpaired Student's *t* test comparing the P830L with other mutants or WT (except S769F and K599A). For simplicity, the *p* values are not indicated in the figures. *F*, Western blot analysis of XBP1 protein in IRE1α$^{-/-}$ MEFs stably expressing WT or mutant IRE1α. Cells were treated with 60 nM Tg for 3 h. *, a nonspecific band. Data are representative of at least two repeats with two independent stable cell lines for each mutant.

Through analysis of IRE1α mutants associated with human somatic cancers (21), our study identifies the interdomain linker region of the cytosolic domain of IRE1α as an important structural determinant for its function. Thus, this region may be used as a potential drug target for small molecules to specifically regulate IRE1α signaling.

EXPERIMENTAL PROCEDURES

Cell Lines and Reagents—IRE1α$^{-/-}$ MEFs were generous gifts from Dr. David Ron (University of Cambridge). T-REx293 cells and T-REx293 cells stably expressing inducible IRE1α-3F6HGFP (16) were gifts from Dr. Peter Walter and Han Li

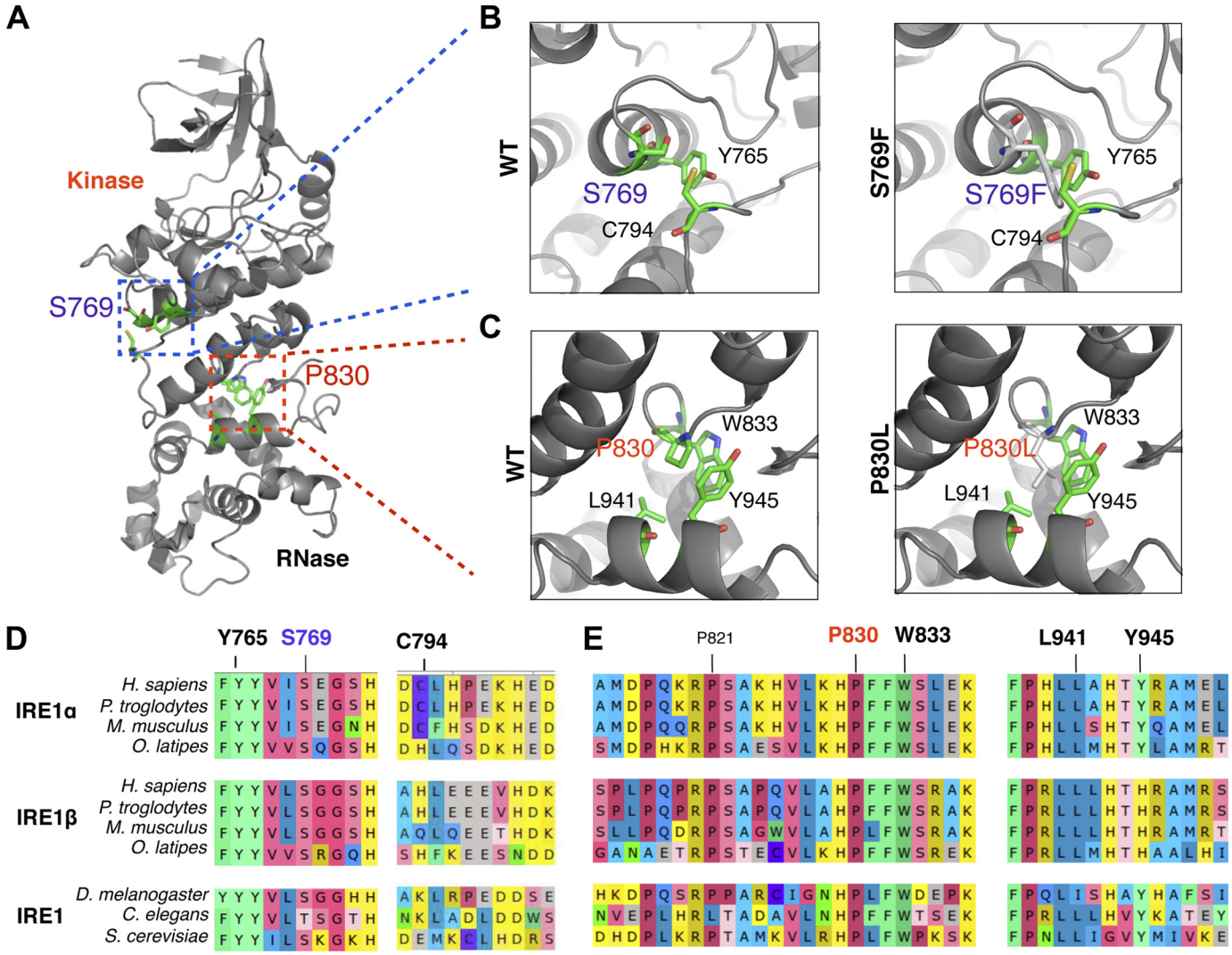

FIGURE 3. **Pro^{830} is located in the highly conserved hydrophobic patch connecting the two cytosolic domains of human IRE1α.** *A*, ribbon diagram of the cytosolic domain of human IRE1α protein (Protein Data Bank accession number 3P23) highlighting two cancer-relevant mutations: S769F (*purple box*) and P830L (*red box*). *B*, close-up view of the Ser^{769} site in WT (*left*) and the structural modeling of the S769F mutant (*right*). Residues (Tyr^{765} and Cys^{794}) that are in close contact with the modeled phenylalanine (*F*) are shown in *sticks*. *C*, close-up view of the Pro^{830} site in WT (*left*) and the structural modeling of the P830L mutant (*right*). Residues (Trp^{833}, Tyr^{945}, and Leu^{941}) that may be in collision with the mutant leucine (*L*) are shown in *sticks*. *P*, proline; *W*, tryptophan; *Y*, tyrosine; *L*, leucine; *S*, serine and *C*, cysteine. *D* and *E*, amino acid sequence alignment showing the conservation of (*D*) Tyr^{765}, Ser^{769}, and Cys^{794} residues and (*E*) Pro^{830}, Trp^{833}, Leu^{941}, and Tyr^{945} residues in IRE1 proteins. Numbers refer to residue positions in human IRE1α protein. *H. sapiens*, human; *P. troglodytes*, chimpanzee; *M. musculus*, mouse; *O. latipes*, fish; *D. melanogaster*, fly; *C. elegans*, worm; *S. cerevisiae*, yeast.

(University of California, San Francisco). HEK293T, T-REx293, and Phoenix cells as described (22) were maintained in DMEM supplemented with 10% FBS (Hyclone) and 1% penicillin/streptomycin. Thapsigargin (Tg; EMD Calbiochem) and stock cycloheximide (Sigma) were dissolved in dimethyl sulfoxide and ethanol, respectively. Cells were treated with Tg at indicated concentrations for indicated times and immediately snap-frozen in liquid nitrogen. Phos-tag was purchased from the NARD Institute (Japan).

Plasmids and Mutagenesis—The pDsRed2-ER (Clontech) plasmid was provided by Dr. Fenghua Hu (Cornell University). pMSCV-IRE1α-HA encoding wild-type (WT) human IRE1α (23) was a gift from Dr. Claudio Hetz (University of Chile). WT IRE1α-3F6HGFP plasmid (16) was provided by Dr. Peter Walter and Han Li. Mutagenesis was performed and sequenced as described (24).

Transfection, Retroviral Transduction, and Stable Cell Lines—HEK293T cells were transfected with plasmids using polyethylenimine (Sigma) as we recently described (24). Cells were snap-frozen in liquid nitrogen 24 h post-transfection followed by Western blotting. To avoid experimental variations due to transfection efficiency, stable IRE1α$^{-/-}$ MEF lines expressing various IRE1α constructs were generated using retroviral transduction as described (22). Stable cell lines were selected in hygromycin (VWR) at 125 μg/ml. Stable cell lines were made and tested independently at least twice.

Analysis of IRE1α Foci Formation—Performed as described (16) with the following modifications. T-REx293 cells were transfected with 0.2–0.5 μg of mutant IRE1α-3F6HGFP plasmid and 1 μg of OG44 (a gift from Dr. Peter Walter) for 24 h followed by selection by 62.5 μg/ml hygromycin for 2–3 weeks. Cells were treated with doxycycline at 5 μg/ml for 24 h to

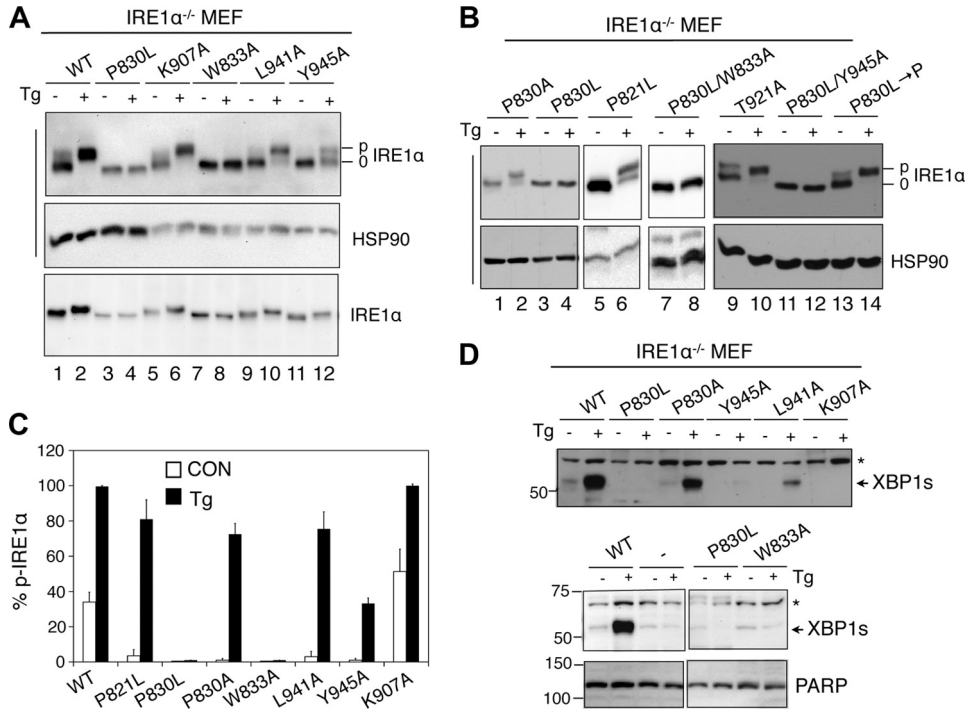

FIGURE 4. **The structural element consisting of Pro^{830}-Trp^{833}-Tyr^{945} is critical for IRE1α function.** *A* and *B*, Western blot analysis of IRE1α in cell lysates of IRE1α$^{-/-}$ MEFs stably expressing WT or mutant IRE1α. Cells were treated with 60 nM Tg for 3 h. *C*, quantitation of *p*-IRE1α in Phos-tag gels shown in *A* and *B*. Results are expressed as mean ± S.E., an average of at least two independent experiments. All *p* values are <0.05 using unpaired Student's *t* test comparing P830L with other mutants or WT (except W833A). For simplicity, the *p* values are not indicated in the figures. *D*, Western blot of XBP1s protein in IRE1α$^{-/-}$ MEFs stably expressing WT or mutant IRE1α. Cells were treated with 60 nM Tg for 4 h. Phos-tag gels are indicated with a *straight line* on the *left side* of the gel. *, a nonspecific band. HSP90, a loading control. Data are representative of at least two repeats for each mutant.

induce expression of IRE1–3F6HGFP followed by Western blotting. In some experiments, cells were plated on a polylysine-coated coverslip in a 6-well plate overnight and transfected with pDsRed2-ER plasmids for 12 h followed by doxycycline (VWR) treatment for 24 h. In some experiments, cells were then treated with Tg at 300 nM for 4 h to induce ER stress. The Prolong Gold Antifade Reagent with DAPI (Invitrogen) was used as mounting medium. Fluorescent microscopic pictures of the T-REx293 were taken with the Zeiss 710 confocal microscope using a 63×/1.4 objective (Cornell Imaging Core Facility).

Structure Analysis of Cytosolic Domains of Yeast and Human IRE1α Proteins—The crystal structure of the cytosolic domain of yeast IRE1α (Protein Data Bank accession number 3FBV) (15) and human IRE1α (Protein Data Bank accession number 3P23) (26) were used for structural analysis of IRE1α mutants.

Cycloheximide Treatment—Stable MEF cell lines with various IRE1α constructs were treated with 100 μg/ml cycloheximide for 0, 6, 9, 12, 16, and 24 h. Cells were then snap-frozen in liquid nitrogen and analyzed by Western blotting.

Western Blotting, Phosphatase Treatment, and Image Quantitation—Preparation of cell lysates, nuclear extract, and Western blotting were performed as we described previously (22, 24). Antibodies used in this study included XBP1 and HSP90 (Santa Cruz Biotechnology), IRE1α (Cell Signaling) and PARP (a gift from Lee Kraus, University of Texas Southwestern Medical Center). Phos-tag gel and phosphatase (λPPase) treatment were performed as described (22, 27, 28). Membranes were routinely strip-reprobed for HSP90 as a position control. Band density was quantitated using the Image Lab software on the ChemiDOC XRS+ system (Bio-Rad) and presented as mean ± S.E. from several independent experiments or as representative data from at least two independent experiments.

RNA Extraction and Xbp1 mRNA Splicing Assay—These experiments were performed as described previously (22).

Statistical Analysis—Results are expressed as mean ± S.E. Comparisons between groups were made by an unpaired two-tailed Student *t* test. $p < 0.05$ was considered statistically significant. All experiments were repeated independently at least twice.

RESULTS

The S769F and P830L Mutations Abolish IRE1α Phosphorylation and Activation—In a recent proteomic screening study, seven mutations (N244S, L474R, R635W, S769F, Q780-stop, and P830L) were identified to be associated with various human cancers (21) (Fig. 1*A*). As they present in tumor cells in one copy (21), their significance in cancer is unclear. Nonetheless, the identification of these mutants allowed us to address how cancer-associated mutations may affect IRE1α structure and function. The relative positions of these mutations in the kinase domain of the active form of yeast IRE1α protein (15), based on homology, are shown in Fig. 1*B*.

To determine the impact of these mutants on IRE1α activity, we generated IRE1α$^{-/-}$ MEF cells stably expressing the mutant proteins and assessed IRE1α phosphorylation in response to ER stress using Phos-tag gels as we recently described (22, 27, 28). Our previous studies have shown that the slower migrating

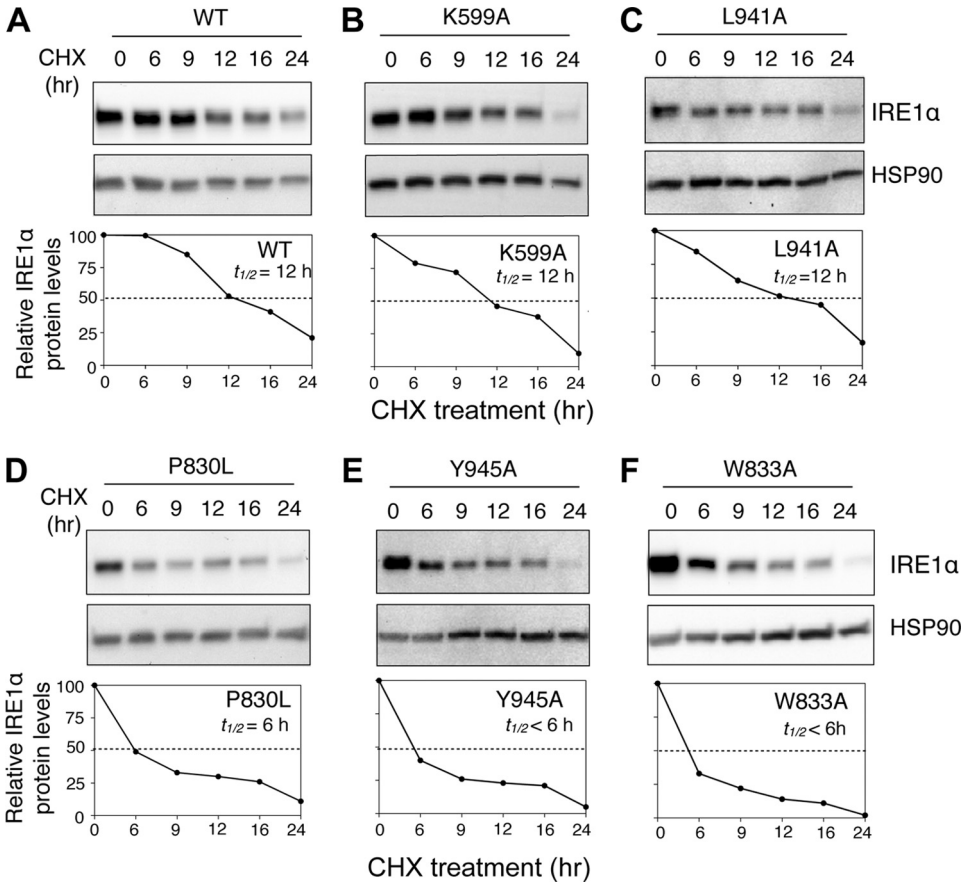

FIGURE 5. **The P830-containing structural linker of IRE1α is important for its stability.** Western blot analysis of IRE1α (*upper*) and quantitation of IRE1α half-life (*lower*) for IRE1α$^{-/-}$ MEFs stably expressing WT or mutant IRE1α. Cells were treated with cycloheximide (*CHX*) for the indicated time. IRE1α protein levels at various time points were normalized to the 0 time point of its own protein. Protein half-life refers to the time at which protein levels reach 50% of the 0 time point. Data are representative of at least two repeats for each mutant. HSP90, loading control.

band on the Phos-tag gel represents the phosphorylated form of IRE1α, and the ratio of phosphorylated to total IRE1α correlates with the amount of ER stress (27, 28). Strikingly, mutation of IRE1α at either S769F or P830L, but not R635W or L474R, abolished IRE1α mobility shift upon Tg treatment, indicative of defective IRE1α kinase activity (Fig. 2*A*, *lanes 7–14*, and Fig. 2*B*, *lanes 1–8*). Of note, we were not able to detect N244S and Q780-stop mutants due to technical reasons. Quantitation of the percent of *p*-IRE1α in total IRE1α from at least two independent experiments is shown in Fig. 2*D*.

It is worth noting that it is necessary to use Phos-tag gels to analyze phosphorylation of IRE1α mutants because *p*-IRE1α did not separate well in regular gels under the same running conditions (Fig. 2, *B* and *C*). The kinase-dead K599A mutant (17) exhibited no IRE1α phosphorylation whereas the dimerization-defective D123P mutant (14) showed a 70% reduction (*lanes 7*, *8*, *10*, and *11*, and Fig. 2*C*). As additional controls, mutations at S548D and T973D had no effect on IRE1α phosphorylation upon ER stress (Fig. 2*A*, *lanes 1–6*). Supporting the notion that the slower migrating band is due to phosphorylation, phosphatase treatment abolished the band-shift in WT IRE1α (Fig. 2*C*, *lane 3*); by contrast, there was no change in the electrophoretic mobility of P830L IRE1α following phosphatase treatment (Fig. 2*C*, *lanes 4–6*).

To examine the effect on RNase activity, we assessed the production of XBP1s protein by Western blotting. K599A completely and D123P partially abolished XBP1s production (Fig. 2*F*, *lower*, *lanes 5–8*) whereas other mutations such as K748A and T973D (Fig. 2*F*, *lower*, *lanes 9–12*) had no effect. XBP1s protein was barely detectable in IRE1α$^{-/-}$ MEFs expressing P830L or S769F (Fig. 2*F*, *upper*, *lanes 9–12*) but was less affected in cells expressing L474R or R635W (Fig. 2*F*, *upper*, *lanes 5–8*). This was also confirmed by RT-PCR analysis of *Xbp1* mRNA splicing (supplemental Fig. S1). Taken together, among the four cancer-associated mutants, our data showed that P830L and S769F mutations had detrimental effects on IRE1α kinase and RNase functions whereas L474R and R635W had no major impact.

Pro^{830} Is Located in a Linker Region Bridging the Two Cytosolic Domains of IRE1α Protein—We then examined the potential effects of the two loss-of-function mutants on IRE1α structure (Fig. 3*A*). Based on the structure of human IRE1α (26), Ser^{769} is located in the kinase domain (Fig. 3*A*). Replacement of the serine with a bulky phenylalanine residue causes sterical collisions with at least two neighboring residues, Tyr^{765} and Cys^{794} (Fig. 3*B*), which may affect the stability and activation of the kinase domain. Although Cys^{794} is not conserved, both Ser^{769} and Tyr^{765} are highly evolutionally conserved (Fig. 3*D*).

Interestingly, Pro^{830} is located at the junction between the kinase and RNase domains (Fig. 3*A*). Further analysis revealed that Pro^{830} may form a highly hydrophobic patch with Trp^{833} and Tyr^{945} or with Leu^{941} on the other side (Fig. 3*C*). Based on

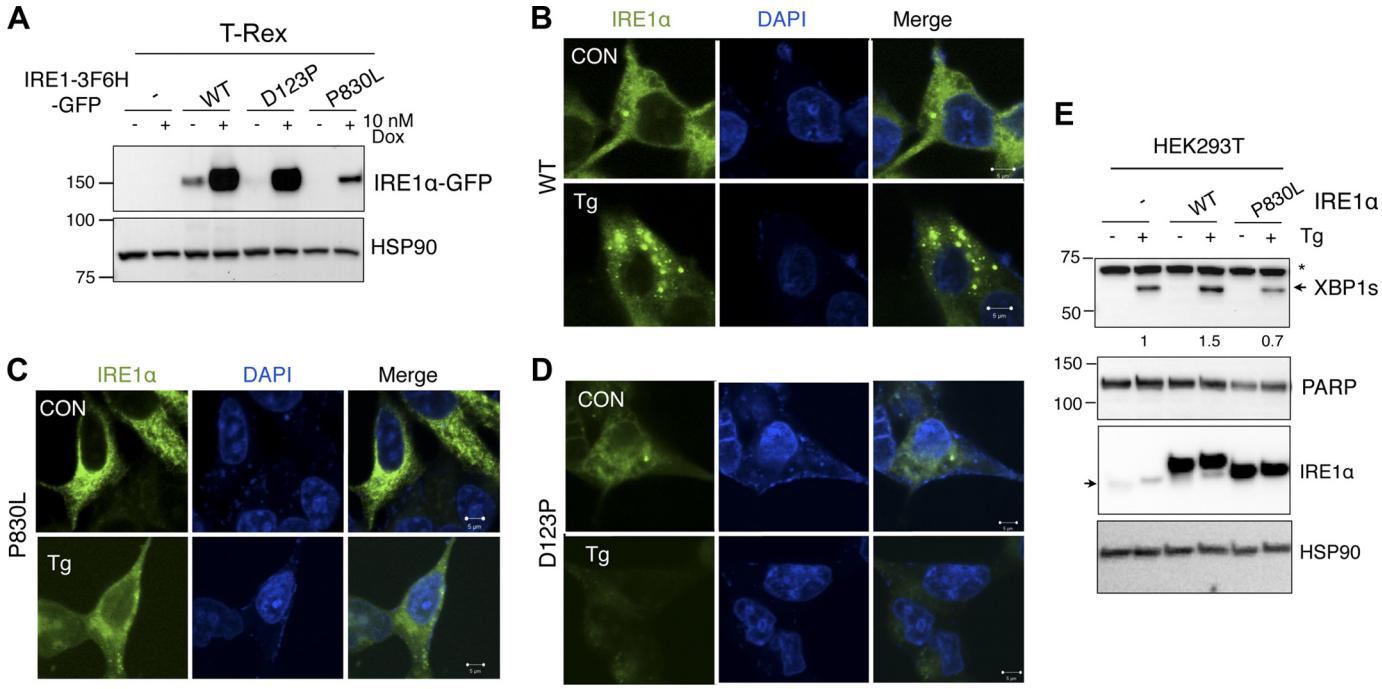

FIGURE 6. **The P830L mutation of IRE1α abolishes its oligomerization in response to ER stress.** *A*, Western blot of IRE1α-GFP proteins in the T-REx293 system. Parental T-REx293 cells (−) or T-REx293 cells stably expressing inducible WT, D123P, or P830L IRE1α proteins were treated with doxycycline (*Dox*) for 24 h followed by Western blotting. *B–D*, confocal microscopic images of IRE1α foci in WT (*B*), P830L (*C*), and D123P (*D*)-expressing cells treated as in *A* with or without 300 nM Tg for 4 h. Images are representatives of >100 cells from three independent experiments. *Scale bar*, 5 μm. *E*, dominant negative effect of P830L. Western blot analysis of XBP1s and IRE1α followed overnight transfection of HEK293T cells with near 100% transfection efficiency. Cells were treated with 300 nM Tg for 4 h prior to harvest. PARP and HSP90, loading controls for XBP1s and IRE1α, respectively. Representative of two independent experiments. *Numbers* shown below the XBP1s blot refer the relative abundance of XBP1s protein (after normalized with PARP). *Arrow* next to the IRE1α blot indicates the endogenous IRE1α band. The ratio of endogenous to exogenous IRE1α protein levels is 1:10.

this, mutation of Pro^{830} to Leu was not favored as the side chain of leucine would contact the Trp^{833} and Tyr^{945} residues (Fig. 3*C*), or Leu^{941} in the other direction (data not shown), and hence, disrupt this structural element. All four residues involved in this structural motif (Pro^{830}, Trp^{833}, Leu^{941}, and Tyr^{945}) were highly conserved in both IRE1α and IRE1β proteins through evolution from yeast to humans (Fig. 3*E*), suggesting that the Pro^{830}-containing structural determinant bridging the two domains of IRE1α may be critical for IRE1α activation in a highly conserved manner. We speculated that understanding the effect of P830L may provide insight into the importance of the region linking the kinase and RNase domains of IRE1α, hereafter termed the "linker." Therefore, in the remainder of this study, we focused on the Pro^{830} residue.

The Structural Element Consisting of Pro^{830}-Trp^{833}-Tyr^{945} Is Critical for IRE1α Function—We next attempted to delineate the effect of this hydrophobic patch consisting of Pro^{830}, Trp^{833}, and Tyr^{945} or Leu^{941} on IRE1α activation by mutagenesis. Interestingly, W833A caused a dramatic defect on IRE1α phosphorylation similar to that of P830L in response to ER stress (Fig. 4*A*, *lanes 7* and *8*), and to a lesser extent, for Y945A (Fig. 4*A*, *lanes 11* and *12*), but not L941A (Fig. 4*A*, *lanes 9* and *10*). To exclude the possibility that the P830L effect was caused by random mutations generated at other sites during mutagenesis, we mutated P830L back to P (P830L→P). Indeed, the P830L→P mutation fully restored the WT phenotype (Fig. 4*B*, *lanes 13* and *14*). Pointing to the importance of the Pro^{830} position, mutation at the nearby P821L, also a highly conserved residue (Fig. 3*E*), had only a minor effect (~20%) on IRE1α phosphorylation (Fig. 4*B*, *lanes 5 and 6*). Moreover, mutation of Pro^{830} to alanine (P830A) caused a much milder defect in IRE1α phosphorylation relative to the P830L mutant, with ~70% of IRE1α being phosphorylated under ER stress (Fig. 4, *B* and *C*, *lanes 1 and 2*).

Next, we asked whether mutating Tyr^{945} or Trp^{833} to a smaller residue such as alanine could reverse the detrimental effect of P830L by accommodating the leucine residue. However, the double mutants of P830L/Y945A or P830L/W833A exhibited the same phenotype as P830L with no IRE1α phosphorylation in response to ER stress (Fig. 4*B*, *lanes 7*, *8*, *11*, and *12*). Quantitation of IRE1α activation in all mutants is shown in Fig. 4*C*.

We then checked the RNase activity of these mutants by assessing the protein levels of XBP1s using Western blotting. Indeed, XBP1 protein levels correlated well with the extent of IRE1α phosphorylation: the P830L, W833A, and Y945A mutations led to no XBP1 production in response to ER stress and to a much lesser extent for L941A and P830A (Fig. 4*D*). As a positive control, RNase-dead K907A mutant (25) with normal IRE1α phosphorylation (Fig. 4*A*, *lanes 5* and *6*) was defective in XBP1 production in response to ER stress (Fig. 4*D*). Taken together, our data showed that three residues, Pro^{830}, Trp^{833}, and Tyr^{945}, not Leu^{941}, likely form a structural linker that is critical for IRE1α function.

The Pro^{830}-containing Structural Linker of IRE1α Is Important for Its Stability—To shed further light on the defects caused by P830L, we examined the stability of IRE1α mutants under basal conditions. $IRE1\alpha^{-/-}$ MEFs stably expressing var-

ious mutant proteins were treated with cycloheximide, an inhibitor of protein synthesis, for the indicated time periods followed by Western blot analysis of IRE1α protein levels. Although K599A had a half-life similar to that of WT protein ($t_{1/2}$ = 12 h; Fig. 5, *A* and *B*), the P830L, W833A, and Y945A mutations dramatically reduced the half-life of IRE1α to 6 h or less (Fig. 5, *D–F*). Pointing to the specificity of these three residues, L941A had no effect on IRE1α stability (Fig. 5*C*). Taken together, these results suggested that P830L, W833A, and Y945A mutations at the linker region had a significant impact on IRE1α protein stability, an effect distinct from the kinase-dead K599A mutation.

The Pro^{830}-containing Structural Linker of IRE1α Is Important for Its Oligomerization—As mammalian IRE1α oligomerizes upon ER stress (16), we next tested the effect of P830L on foci formation. To this end, we used an inducible system to detect IRE1α foci formation in T-REx293 cells (16) (Fig. 6*A*). Using co-expression of ER-localized dsRed encoded in the pDsRed2-ER plasmid, we first confirmed that exogenous WT and mutant IRE1α proteins were predominantly localized to the ER (supplemental Fig. S2). In line with a previous study (16), foci formation peaked in cells expressing WT-IRE1α protein upon 4-h treatment of 300 nM TG (Fig. 6*B* and data not shown). Interestingly, unlike WT IRE1α, P830L failed to form foci upon ER stress (Fig. 6*C*) as did the dimerization-defective D123P IRE1α (Fig. 6*D*). Thus, the Pro^{830}-containing structural linker of IRE1α affects its oligomerization in response to ER stress.

To test whether mutant IRE1α protein would have a dominant negative effect on endogenous IRE1α protein, we transfected mutant proteins into HEK293T cells and tested for an ER stress response. Surprisingly, despite being expressed 10-fold more than endogenous protein levels, exogenous mutant proteins failed to reduce IRE1α activity significantly as assessed by XBP1 protein levels (Fig. 6*E*). Thus, the P830L mutant does not act as a dominant negative mutation but rather may serve as a loss-of-function mutation.

DISCUSSION

This is the first study addressing how cancer-associated IRE1α mutations affect its structure and function. Here, we have identified an important structural element that is critical for the function of IRE1α. This structural linker consisting of Pro^{830}, Trp^{833}, and Tyr^{945} bridges the cytosolic kinase and RNase domains of IRE1α protein. Disturbance of this linker structure abolishes the activities of both functional domains and prevents IRE1α foci formation in response to ER stress. This mechanism is likely to be evolutionarily conserved as these three residues are highly conserved from yeast to humans. Although it remains unclear how P830L may affect tumor development *in vivo* (which is not the focus of this study), this study demonstrates that the P830L mutation is deleterious for IRE1α stability and function.

How the folding and activation of the two cytosolic domains of IRE1α are coupled *in vivo* remains unclear. Currently, one prevailing model is that the activation of the RNase domain of IRE1α depends on the trans-autophosphorylation of its adjacent kinase domain following dimerization or oligomerization (1, 18). Efforts to understand this phosphorylation-mediated regulatory event further are hampered by an incomprehensive knowledge of all of the specific phosphorylated residues on mammalian IRE1α protein. In yeast, an estimated 17 Ser/Thr residues located at both the activation loop and the adjacent αEF-αF loop are believed to be phosphorylated under ER stress (15). Although we predict that trans-autophosphorylation of mammalian IRE1α protein is not likely to be as extensive as in yeast, as indicated by a single shift in the Phos-tag-based Western blots (22, 27, 28), the identities and the importance of these possible phosphorylation events on mammalian IRE1α activation remain an interesting question.

Our data suggest that the Pro^{830}-Trp^{833}-Tyr^{945} residues in the IRE1α hydrophobic core are important for its folding and activation. This linker region affects not only the activities of the kinase and RNase domains, but also its half-life and the ER stress-induced oligomerization. The effect of Pro^{830}-related mutations on IRE1α function is indeed more severe than the kinase-dead K599A or the dimerization-defective D123P mutants, suggesting that Pro^{830}-related mutations may interfere with the folding process of IRE1α protein. How we can translate this finding to therapeutic purposes require further studies.

Acknowledgments—We thank the Qi laboratory for helpful discussions; Dr. C. J. Bayles for the help with confocal microscopy; Drs. C. Hetz, F. Hu, L. Kraus, H. Li, D. Ron, and P. Walter for reagents.

REFERENCES

1. Ron, D., and Walter, P. (2007) *Nat. Rev. Mol. Cell Biol.* **8,** 519–529
2. Cox, J. S., Shamu, C. E., and Walter, P. (1993) *Cell* **73,** 1197–1206
3. Mori, K., Ma, W., Gething, M. J., and Sambrook, J. (1993) *Cell* **74,** 743–756
4. He, Y., Sun, S., Sha, H., Liu, Z., Yang, L., Xue, Z., Chen, H., and Qi, L. (2010) *Gene Expr.* **15,** 13–25
5. Cox, J. S., and Walter, P. (1996) *Cell* **87,** 391–404
6. Sidrauski, C., and Walter, P. (1997) *Cell* **90,** 1031–1039
7. Travers, K. J., Patil, C. K., Wodicka, L., Lockhart, D. J., Weissman, J. S., and Walter, P. (2000) *Cell* **101,** 249–258
8. Calfon, M., Zeng, H., Urano, F., Till, J. H., Hubbard, S. R., Harding, H. P., Clark, S. G., and Ron, D. (2002) *Nature* **415,** 92–96
9. Lee, K., Tirasophon, W., Shen, X., Michalak, M., Prywes, R., Okada, T., Yoshida, H., Mori, K., and Kaufman, R. J. (2002) *Genes Dev.* **16,** 452–466
10. Yoshida, H., Matsui, T., Yamamoto, A., Okada, T., and Mori, K. (2001) *Cell* **107,** 881–891
11. Liu, C. Y., Schröder, M., and Kaufman, R. J. (2000) *J. Biol. Chem.* **275,** 24881–24885
12. Liu, C. Y., Wong, H. N., Schauerte, J. A., and Kaufman, R. J. (2002) *J. Biol. Chem.* **277,** 18346–18356
13. Liu, C. Y., Xu, Z., and Kaufman, R. J. (2003) *J. Biol. Chem.* **278,** 17680–17687
14. Zhou, J., Liu, C. Y., Back, S. H., Clark, R. L., Peisach, D., Xu, Z., and Kaufman, R. J. (2006) *Proc. Natl. Acad. Sci. U.S.A.* **103,** 14343–14348
15. Korennykh, A. V., Egea, P. F., Korostelev, A. A., Finer-Moore, J., Zhang, C., Shokat, K. M., Stroud, R. M., and Walter, P. (2009) *Nature* **457,** 687–693
16. Li, H., Korennykh, A. V., Behrman, S. L., and Walter, P. (2010) *Proc. Natl. Acad. Sci. U.S.A.* **107,** 16113–16118
17. Tirasophon, W., Welihinda, A. A., and Kaufman, R. J. (1998) *Genes Dev.* **12,** 1812–1824
18. Lee, K. P., Dey, M., Neculai, D., Cao, C., Dever, T. E., and Sicheri, F. (2008) *Cell* **132,** 89–100
19. Han, D., Lerner, A. G., Vande Walle, L., Upton, J. P., Xu, W., Hagen, A., Backes, B. J., Oakes, S. A., and Papa, F. R. (2009) *Cell* **138,** 562–575
20. Papa, F. R., Zhang, C., Shokat, K., and Walter, P. (2003) *Science* **302,**

1533–1537
21. Greenman, C., Stephens, P., Smith, R., Dalgliesh, G. L., Hunter, C., Bignell, G., Davies, H., Teague, J., Butler, A., Stevens, C., Edkins, S., O'Meara, S., Vastrik, I., Schmidt, E. E., Avis, T., Barthorpe, S., Bhamra, G., Buck, G., Choudhury, B., Clements, J., Cole, J., Dicks, E., Forbes, S., Gray, K., Halliday, K., Harrison, R., Hills, K., Hinton, J., Jenkinson, A., Jones, D., Menzies, A., Mironenko, T., Perry, J., Raine, K., Richardson, D., Shepherd, R., Small, A., Tofts, C., Varian, J., Webb, T., West, S., Widaa, S., Yates, A., Cahill, D. P., Louis, D. N., Goldstraw, P., Nicholson, A. G., Brasseur, F., Looijenga, L., Weber, B. L., Chiew, Y. E., DeFazio, A., Greaves, M. F., Green, A. R., Campbell, P., Birney, E., Easton, D. F., Chenevix-Trench, G., Tan, M. H., Khoo, S. K., Teh, B. T., Yuen, S. T., Leung, S. Y., Wooster, R., Futreal, P. A., and Stratton, M. R. (2007) *Nature* **446,** 153–158
22. Sha, H., He, Y., Chen, H., Wang, C., Zenno, A., Shi, H., Yang, X., Zhang, X., and Qi, L. (2009) *Cell Metab.* **9,** 556–564
23. Hetz, C., Bernasconi, P., Fisher, J., Lee, A. H., Bassik, M. C., Antonsson, B., Brandt, G. S., Iwakoshi, N. N., Schinzel, A., Glimcher, L. H., and Korsmeyer, S. J. (2006) *Science* **312,** 572–576
24. Chen, H., and Qi, L. (2010) *Biochem. J.* **429,** 95–102
25. Tirasophon, W., Lee, K., Callaghan, B., Welihinda, A., and Kaufman, R. J. (2000) *Genes Dev.* **14,** 2725–2736
26. Ali, M. M., Bagratuni, T., Davenport, E. L., Nowak, P. R., Silva-Santisteban, M. C., Hardcastle, A., McAndrews, C., Rowlands, M. G., Morgan, G. J., Aherne, W., Collins, I., Davies, F. E., and Pearl, L. H. (2011) *EMBO J.* **30,** 894–905
27. Yang, L., Xue, Z., He, Y., Sun, S., Chen, H., and Qi, L. (2010) *PLos ONE* **5,** e11621
28. Qi, L., Yang, L., and Chen, H. (2011) *Methods Enzymol.* **490,** 137–146

A Conserved Structural Determinant Located at the Interdomain Region of Mammalian Inositol-requiring Enzyme 1 α

Zhen Xue, Yin He, Kaixiong Ye, Zhenglong Gu, Yuxin Mao and Ling Qi

J. Biol. Chem. 2011, 286:30859-30866.
doi: 10.1074/jbc.M111.273714 originally published online July 13, 2011
